JOURNAL OF Materials CHEMISTRY

Charge-transfer salts of $M(mnt)_2$ (M = Ni, Pd, Pt, Au) with BDNT: ferromagnetic interactions in conductive $(BDNT)_2$–$[Ni(mnt)_2]$

M. Uruichi,[a] K. Yakushi,[a] Y. Yamashita[a]* and J. Qin[b]

[a]*Institute for Molecular Science, Myodaiji, Okazaki, Aichi 444, Japan*
[b]*Department of Chemistry, Wuhan University, Wuhan 430072, China*

Charge-transfer salts between BDNT and $M(mnt)_2$ (M = Ni, Pd, Pt, and Au) have been prepared by mixing BDNT–$(SbCl_6)_2$ and $(TBA)_2$–$[M(mnt)_2]$ and by electrochemical oxidation of BDNT in TBA–$[M(mnt)_2]$ solution. Almost all powdery samples of (1 : 1) salts show high electrical conductivity. The valence of $M(mnt)_2$ was determined to be -1 by the CN stretching mode, which means that the valence of BDNT is $+0.5$, $+1$, or $+2$. Their crystal structures are not known except for the low-conductive BDNT–$[Au(mnt)_2]_2$, in which $Au(mnt)_2$ forms dimers which are arranged in crisscross stacks. Among these compounds, $(BDNT)_2$–$[Ni(mnt)_2]$ exhibits a ferromagnetic interaction with $|J| = 3.4$ K. It is concluded from the EPR experiment that $[Ni(mnt)_2]^-$ is responsible for the ferromagnetic interaction.

BDNT {4,9-bis(1,3-benzodithiol-2-ylidene)-4,9-dihydronaphtho[2,3-*c*][1,2,5]thiadiazole} (see Fig. 1) is a newly synthesized, butterfly-shaped electron donor molecule, and gives stable solid monocation and dication salts. BDNT exhibits a unique electrochemical property in that the first and second oxidation potentials are very close so they are not resolved in the cyclic voltammetric experiment. From the analysis of the width of the oxidation wave, the difference between the first and second oxidation potentials, ΔE, has been estimated to be 0.024 eV.[1] The exact one-step two-electron oxidation leads to the possibility of a negative-*U* state in the solid state,[2] because the monocation is less stable than the neutral molecule and the dication. The negative-*U* state has not yet been found in organic charge-transfer crystals; the search for such a material is the on-going program in our laboratory. We have characterized the spectroscopic properties of $BDNT^0$, $BDNT^+$, and $BDNT^{2+}$ in solution and in the solid state,[3] and have examined the electronic and vibronic structures of *m*-BDNT–PF_6, which is a conventional positive-*U* compound.[4] The combination of BDNT with large planar anions may provide new segregate-stacked BDNT charge-transfer salts, since BDNT is not planar and thus prevents the formation of a mixed-stack structure. Bis(maleonitriledithiolate)metalate $M(mnt)_2$ (see Fig. 1) gives stable monoanions and dications and its charge-transfer salts have been extensively studied from the viewpoint of conductivity and magnetism.[5] In this paper, we will present the solid-state properties of the charge-transfer salts of BDNT with $[M(mnt)_2]^-$.

Experimental

Dark brown powders were precipitated by mixing equimolar acetonitrile solutions of BDNT–$(SbCl_6)_2$ with $(TBA)_2$–$[M(mnt)_2]$ (M = Ni, Pd, Pt). These precipitates were washed first with acetonitrile and then with dichloromethane. To obtain single crystals, we used a diffusion method and an electrochemical method. In the former method, we used an H-tube and acetonitrile was the solvent. After two weeks, very small polycrystals were grown in the midpoint of the arms of the H-tube. In the latter method, BDNT was dissolved in the anode compartment of a U-tube with a glass filter, a dichloromethane solution of $(TBA)_2$–$[M(mnt)_2]$ being the electrolyte solution. The products were the same as those of the diffusion method, and single crystals were not obtained (Found: C, 50.35; H, 1.26; N, 8.07%. Calc. for $(C_{24}H_{12}N_2S_5)_2$–$C_8N_4S_4Ni$: C, 51.09; H, 1.82; N, 8.51%. Found: C, 43.67; H, 1.71, N, 9.11%. Calc. for $C_{24}H_{12}N_2S_5$–$C_8N_4S_4Pd$: C, 43.90; H, 1.38; N, 9.60%. Found: C, 39.10; H, 1.57; N, 7.95%. Calc. for $C_{24}H_{12}N_2S_5$–$C_8N_4S_4Pt$: C, 39.87; H, 1.25; N, 8.72%). The complex between BDNT and $Au(mnt)_2$ was obtained by mixing acetonitrile solutions of BDNT–$(SbCl_6)_2$ and TBA–$[Au(mnt)_2]$ in a 1 : 2 ratio. Single crystals were found in the black powder precipitate. Both the single crystals and the powder were found to be the 1 : 2 complex of BDNT and $Au(mnt)_2$, as determined by chemical analysis and crystal structure analysis (black powder: Found: C, 32.67; H, 1.60; N, 7.33%. Calc. for $C_{24}H_{12}N_2S_5$–$(C_8N_4S_4Au)_2$: C, 33.29; H, 0.84; N, 9.70%). The electrochemical oxidation of BDNT in a dichloromethane solution of TBA–$[Au(mnt)_2]$ provided a black powder of the 1 : 1 complex (Found: C, 41.56; H, 1.67; N, 8.16%. Calc. for $C_{24}H_{12}N_2S_5$–$C_8N_4S_4Au$: C, 39.79; H, 1.25; N, 8.70%).

The IR spectra of the powder samples dispersed in KBr disks were measured on a Jasco VM-7 FTIR spectrometer. Powder X-ray diffraction patterns were obtained on a MAC Science MXP^{3}VA instrument. The dc electrical resistivities of the polycrystalline samples were measured using a four-probe method with a Quantum Design PPMS and Digital Voltmeter, Keithley 2001. The resistivity of a single crystal of BDNT–$[Au(mnt)_2]_2$ was measured by the two-probe method using the same instrument. Silver paint and 20 μm gold wires were used for the electrical contact with the electrodes. The magnetic susceptibilities of powder samples were measured with a SQUID magnetometer (Quantum Design, MPMS-2 and MPMS-7) in the temperature range 2–300 K with applied fields of 0.2 T and 1 T. The diamagnetic contribution to the magnetic susceptibility was estimated from the temperature-dependent susceptibility of BDNT (-3.29×10^{-4} emu mol^{-1}), $(TBA)_2$–$M(mnt)_2$ [M = Ni (-4.37×10^{-4} emu mol^{-1}), Pd (-5.98×10^{-4} emu mol^{-1}), Pt (-4.78×10^{-4} emu mol^{-1})], TBA–$Au(mnt)_2$ (-3.78×10^{-4} emu mol^{-1}), and TBA–BF_4

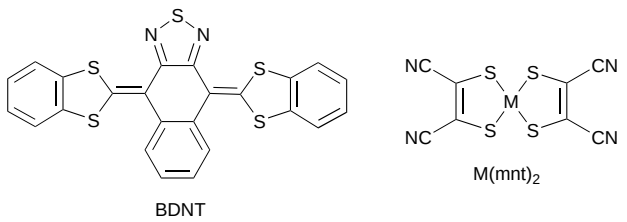

Fig. 1 Structural formulae of BDNT and $M(mnt)_2$

(-2.08×10^{-4} emu mol^{-1}). The molar diamagnetic susceptibility of BF_4 (-0.39 emu mol^{-1}) was calculated by Pascal's law. EPR measurements were carried out on a Brüker ESP-300E, equipped with a Oxford Instruments EPR900 cryostat combined with an ITC4 temperature controller.

Results and Discussion

Electrical properties

Table 1 shows the electrical conductivities of the powdery samples measured by the four-probe method. All 1:1 salts give high conductivities and low activation energies, which is surprising, since only $(TTT)_2$–$[Pt(mnt)_2]$,[6] $(perylene)_2$–$[Ni(mnt)_2]$,[7] and $(perylene)_2$–$[Pt(mnt)_2]$[8] show such high conductivity values among the charge-transfer complexes of $M(mnt)_2$ with planar organic donor molecules. Furthermore, partially oxidized donor molecules take part in the high conductivity in these complexes, whereas (BDNT)–$[M(mnt)_2]$ (M = Pd, Pt, Au) has a 1:1 composition. Therefore, the evaluation of the charge (valence) of BDNT and $M(mnt)_2$ is important.

The vibrational bands observed in the powdery samples were compared with those of BDNT, BDNT–PF_6, BDNT–$(PF_6)_2$, TBA–$[M(mnt)_2]$ and $(TBA)_2$–$[M(mnt)_2]$. The normal-coordinate analysis of $[Ni(mnt)_2]^{n-}$ ($n=1, 2$) was conducted by Schlapfer and Nakamoto.[9] They pointed out that the C=C stretching mode is sensitive to the charge (valence) of $Ni(mnt)_2$, appearing at 1435 cm^{-1} in $[Ni(mnt)_2]^-$ and 1485 cm^{-1} in $[Ni(mnt)_2]^{2-}$. For BDNT, strong characteristic bands are found at 1509 cm^{-1} in $BDNT^0$, at 1406 and 745 cm^{-1} in $BDNT^+$, and at 1381 and 768 cm^{-1} in $BDNT^{2+}$.[3] However, the vibrational bands of BDNT and $M(mnt)_2$ are overlapped in the spectral region of the characteristic modes. We can qualitatively say that the IR spectrum in the 400–1800 cm^{-1} region resembles very closely that of $BDNT^+$. The well isolated CN stretching mode is the unique mode which can be used for the evaluation of the valence of $M(mnt)_2$. Best *et al.* have studied the relationship between the CN stretching modes and the charge (-1 to -3) of $M(mnt)_2$.[10] The CN stretching mode shifts by about 15 cm^{-1} to the low wavenumber side with increasing the charge from -1 to -2. Comparisons are shown in Table 2 along with other $M(mnt)_2$ salts. We conclude that all $M(mnt)_2$ salts, except that of $Au(mnt)_2$ in a 1:2 complex, have a charge of nearly -1, although it is difficult to quantitatively estimate the valence of $M(mnt)_2$. In BDNT–$[Au(mnt)_2]_2$, the combination of the valences is $[+1, -0.5]$ or $[+2, -1]$. The magnetic susceptibility suggests the former. The similarity of the CN stretching modes between the 1:1 and 1:2 $Au(mnt)_2$ salts may be ascribed to the insensitivity of the charge from -1 to 0. The 2:1 and 1:1 charge-transfer salts of BDNT exhibit relatively high electrical conductivities: the intrinsic Mott–Hubbard semiconductor *m*-BDNT–PF_6 has a room temperature conductivity of 3×10^{-3} S cm^{-1} with an activation energy of 0.2 eV,[4] while another modification, *o*-BDNT–PF_6, has a room-temperature conductivity of 0.4 S cm^{-1} with an activation energy of 0.05 eV.[11] The high conductivity of the latter comes from a small deviation from the exact 1:1 ratio.[11] Some 1:1 charge-transfer salts of $M(mnt)_2$ with alkali metals also show rather high conductivity values around 1 S cm^{-1}, although many other 1:1 salts shows low conductivity values, typically less than 10^{-5} S cm^{-1}.[5] Since the conductivity is rather high, the BDNT and/or $M(mnt)_2$ seems to have a uniformly stacked column. As will be discussed later, the BDNT column is responsible for the conductivity. We will return to this problem when we discuss the EPR and magnetic properties.

Table 1 Room temperature resistivity and activation energy

compound[a]	σ_{RT}/S cm^{-1}	activation energy/eV
$(BDNT)_2$–$[Ni(mnt)_2]$ (p)	0.5	0.06
BDNT–$[Pd(mnt)_2]$ (p)	1.3	0.043
BDNT–$[Pt(mnt)_2]$ (p)	2.5	0.036
BDNT–$[Au(mnt)_2]$ (p)	0.4	0.05
BDNT–$[Au(mnt)_2]_2$ (p)	1×10^{-2}	0.10
BDNT–$[Au(mnt)_2]_2$ (s)	1×10^{-7}	0.19

[a]p: powder, s: single crystal.

Table 2 CN stretching mode of $[M(mnt)_2]^{n-}$ [a]

		$[M(mnt)_2]^-$	$[M(mnt)_2]^{2-}$	BDNT complex
$Ni(mnt)_2$	solution	**2211**, 2226(sh)	**2195**, 2213(sh)	
	Et_4N^+	2194(sh), **2210**	**2195**, 2205(sh)	
	Bu_4N^+		**2197**, 2216(sh)	
	BDNT			**2211**
$Pd(mnt)_2$	solution	**2212**	**2198**, 2233(sh)	
	Bu_4N^+		**2195**, 2215(sh)	
	BDNT			**2207**
$Pt(mnt)_2$	solution	2204(sh), **2215**	2189(sh), **2200**	
	Bu_4N^+		2188(sh), **2197**	
	BDNT			**2209**
$Au(mnt)_2$	solution	**2213**, 2226(sh)	**2195**	
	Bu_4N^+	**2209**, 2222		
	BDNT			**2207**
	(1:1), (1:2)			2220

[a]Numbers in bold type indicate the stronger intensity.

Crystal structure

All the complexes show sharp powder X-ray diffraction peaks, which indicates good crystallinity. Among these complexes, we succeeded in growing single crystals only for the low-conductive 1:2 salts of BDNT and $Au(mnt)_2$. First, a powdery sample of BDNT–$[Au(mnt)_2]_2$ gives a quite different X-ray diffraction pattern from a single crystal BDNT–$[Au(mnt)_2]_2$, in which BDNT is not butterfly-shaped but twisted. The twisted molecular structure is characteristic of the BDNT dication,[12] and the dimer of $Au(mnt)_2$ is stacked in a criss-cross way, from which high conductivity cannot be expected. So the high conductivity of the 1:2 powdery sample is attributed to the difference in structure and valence. The X-ray diffraction patterns of BDNT–$[Au(mnt)_2]$ and BDNT–$[Pt(mnt)_2]$ are very similar, so they are probably isostructural. BDNT–$[Pd(mnt)_2]$ and $(BDNT)_2$–$[Ni(mnt)_2]$ are different from the above two complexes as well as from each other. As a result, all of these diffraction patterns are different from that of BDNT–$[Au(mnt)_2]_2$, the structure of which is given in the Appendix.

Magnetic properties

Before describing the magnetic properties of the charge-transfer salts, let us add a brief comment on the electronic configuration of each component. $BDNT^+$ is a radical cation and $[M^{II}(mnt)_2]^-$ (M = Ni, Pd, Pt) are radical anions, while $[Au^{III}(mnt)_2]^-$ is a diamagnetic anion. The molar diamagnetic susceptibility was estimated as -3.29×10^{-4} emu mol^{-1} for BDNT, -1.00×10^{-4} emu mol^{-1} for $[Ni(mnt)_2]^{2-}$, -2.60×10^{-4} emu mol^{-1} for $[Pd(mnt)_2]^{2-}$, -1.40×10^{-4} emu mol^{-1} for $[Pt(mnt)_2]^{2-}$, and -2.09×10^{-4} emu mol^{-1} for $[Au(mnt)_2]^-$. So the charge-transfer salts constitute two magnetic components except for the 1:1 $Au(mnt)_2$ salt and 1:2 single crystal. The magnetic susceptibilities of all BDNT complexes are shown in Fig. 2. It is clear at a first glance that the Curie constant of $(BDNT)_2$–$[Ni(mnt)_2]$ is much larger than those of the other salts. The susceptibility curves were

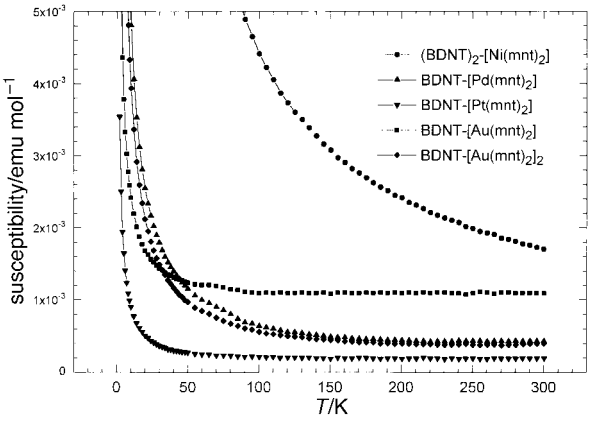

Fig. 2 Static magnetic susceptibilities of charge-transfer salts, BDNT–M(mnt)$_2$. BDNT–[Au(mnt$_2$]$_2$ is a powdery modification.

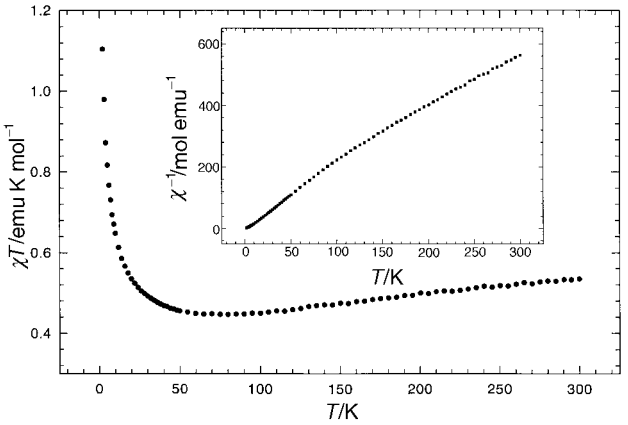

Fig. 3 χT and χ^{-1} *vs.* T plots of (BDNT)$_2$–[Ni(mnt)$_2$]. Both shows antiferromagnetic behavior when $T>150$ K, while ferromagnetic behavior when $T<100$ K.

fitted using the following equation

$$\chi(T)=\frac{C}{T-\theta}+\chi_c$$

These parameters are listed in Table 3 along with the g-values and linewidths of the EPR signals. Except for (BDNT)$_2$–[Ni(mnt)$_2$], the numbers of unpaired electrons per molecule (N/N_A) calculated from the Curie constants are much smaller than unity, indicating antiferromagnetic interactions. When χT is plotted against T, only (BDNT)$_2$–[Ni(mnt)$_2$] shows ferromagnetic behavior at low temperature. From the Curie constants, these salts are classified into three types: N/N_A is nearly unity for Ni(mnt)$_2$, *ca.* 10% for Pd(mnt)$_2$ and Pt(mnt)$_2$, and less than 4% for Au(mnt)$_2$ 1:1 and 1:2 salts. The EPR signal of BDNT–[Au(mnt)$_2$] exhibits a well defined orthorhombic lineshape at 3.6 K with principal g-values shown in Table 3, which are very similar to those of *m*-BDNT–PF$_6$, $g_1=2.0039$, $g_2=2.0051$, and $g_3=2.0105$.[11] In this compound the Curie component is unambiguously attributed to isolated BDNT$^+$ at the lattice defect sites. The magnitude of the temperature independent term is similar to those of the simple salts [$(1–2)\times10^{-4}$ emu mol^{-1}] of BDNT such as BDNT–X (X = PF$_6^-$, ClO$_4^-$, AsF$_6^-$, and Br$_3^-$), in which BDNT makes a one-dimensional column with antiferromagnetic interactions.[11] This means that Au(mnt)$_2$ does not contribute to the magnetic properties, which is consistent with the valence of [Au(mnt)$_2$]$^-$ indicated by the CN stretching mode. Although the Curie component is small, BDNT–[Au(mnt$_2$]$_2$ has a large T-independent term. This might suggest the presence of the paramagnetic species [Au(mnt)$_2$]$^{0.5-}$ or [Au(mnt)$_2$]^0 in addition to BDNT$^+$. In this context, the much weaker EPR signal of a single crystal of BDNT–[Au(mnt$_2$]$_2$ is reasonable, since both BDNT^{2+} and [Au(mnt)$_2$]$^-$ are diamagnetic ions (deduced from the crystal structure analysis). BDNT–[Pd(mnt)$_2$] and BDNT–[Pt(mnt)$_2$] have Curie constants which are too large for them to be regarded as lattice

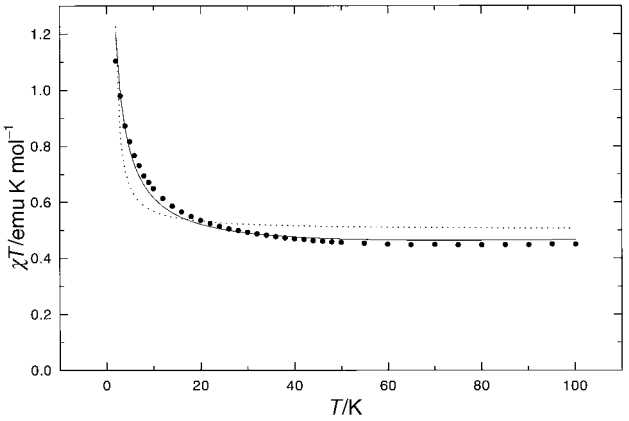

Fig. 4 χT data (●) and least-squares fitting by Curie–Weiss (-----) and 1D ferromagnetic models (—) of (BDNT)$_2$–[Ni(mnt)$_2$]

defect structures. EPR suggests that the paramagnetic species come from [Pd(mnt)$_2$]$^+$ for BDNT–[Pd(mnt)$_2$] and from BDNT$^+$ for BDNT–[Pt(mnt)$_2$]. The origin of this paramagnetism is not clear at the moment.

Fig. 3 shows χT and χ^{-1} plots *vs.* temperature of (BDNT)$_2$–[Ni(mnt)$_2$], measured at $B=0.2$ T. The curve χ^{-1} indicates a continuous change of the magnetic behavior around 125 K (100–150 K) from antiferromagnetic to ferromagnetic behavior. However, the high-temperature region ($T>20$ K) can be well fitted by eqn. (1) with the fitting parameters shown in Table 3. The χT plot shows clearly the ferromagnetic interaction below 100 K. The low temperature region of χT was fitted by the least-squares calculation of the 1D ferromagnetic model[13] with $C=0.43$ and $|J|=3.4$ K much better than by the Curie–Weiss model with $C=0.49$ and $\theta=1.2$ K, as shown in Fig. 4. However, the sharp increase in χT below 20 K

Table 3 Magnetic properties

	C/emu K mol^{-1}	N/N_A	θ/K	χ_c/emu mol^{-1}	g-value at 3.6 K	ΔH/G at 300 K
Ni(2:1)[a]	0.397	1.01	3.8	4.5×10^{-4}	$g_{BDNT}=2.004$	13
					$g_{Ni}=2.043$	350
Pd(1:1)	0.0386	0.10	−0.43	2.1×10^{-4}	$g_{av}=2.019$	140
Pt(1:1)	0.0495	0.13	−0.61	1.9×10^{-4}	$g_{av}=2.006$	13
Au(1:1)	0.0077	0.02	−0.26	1.4×10^{-4}	$g_1=2.003$	
					$g_2=2.005$	17
					$g_3=2.009$	
Au(1:2) powder	0.0147	0.04	−0.35	1.0×10^{-3}	$g_{av}=2.006$	14

[a]M(m:n): (BDNT)$_m$–[M(mnt)$_2$]$_n$.

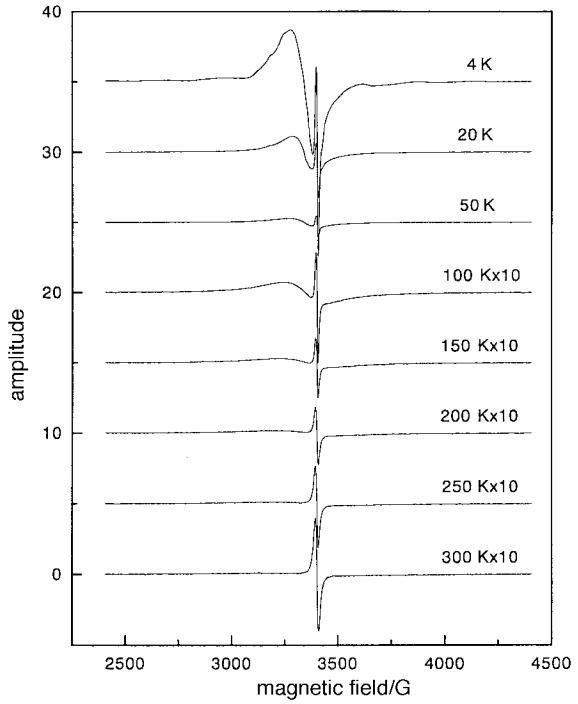

Fig. 5 Evolution of the EPR signal of $Ni(mnt)_2$ in $(BDNT)_2$–$[Ni(mnt)_2]$. $Ni(mnt)_2$ is responsible for the ferromagnetic interaction.

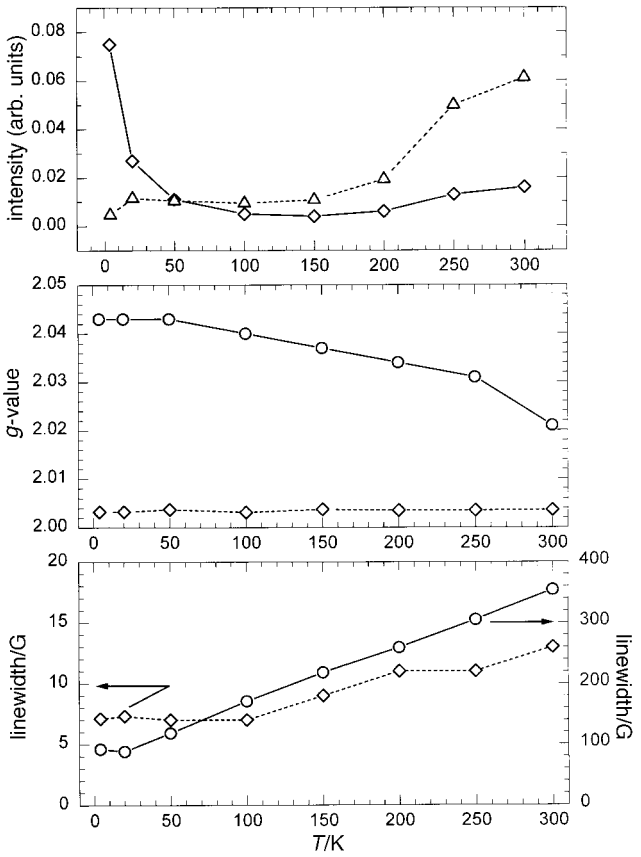

Fig. 6 Temperature dependence of the EPR properties of BDNT and $Ni(mnt)_2$. Top panel: temperature dependence of the EPR intensity of BDNT (diamonds) and intensity ratio (triangles). The intensity of $Ni(mnt)_2$ is much larger than BDNT in whole temperature range. Middle panel: temperature dependence of the *g*-values of BDNT (diamonds) and $Ni(mnt)_2$ (circles). Bottom panel: temperature dependence of the linewidths of BDNT (diamonds) and $Ni(mnt)_2$ (circles).

is slower than the 1D ferromagnetic model. No hysteresis was observed at 2 K in the magnetization curve, which deviates from the linear increase *vs.* magnetic field at 0.4 T, levels off at 3 T but does not saturate, and increases linearly up to 8 T. The magnetization at maximum field (8 T) is 0.8 μ_B. The magnetization curve at low magnetic field is much sharper than the Brillouin function of $S=1/2$, which suggests short-range ordering of ferromagnetic clusters. The linear increase of χT in the high temperature region indicates a T-independent or weakly dependent component.

The EPR spectrum of $(BDNT)_2$–$[Ni(mnt)_2]$ constitutes of broad and sharp signals, the evolution of the former being shown in Fig. 5. It is reasonable to assign the broad and sharp signals to $[Ni(mnt)_2]^-$ and $BDNT^+$, respectively. These two signals were deconvoluted into two Lorentzian signals. The separate appearance of these two signals indicates weak coupling between the BDNT spin and the $Ni(mnt)_2$ spin. The integrated intensity of the broad signal is much stronger than that of the sharp signal as shown in the top panel of Fig. 6 (see the intensity ratio). For example, the intensity ratio of $BDNT/Ni(nmt)_2$ is 0.06 at 300 K and it decreases to less than 0.02 below 200 K. So $Ni(mnt)_2$ takes part in the magnetic properties shown in Fig. 2 and 3, and the contribution of BDNT paramagnetism is negligible in the analysis of the static magnetic susceptibility curve.

Very similar magnetic behavior has been observed,[14] by Cambridge and North Wales research groups, for NH_4–$Ni(mnt)_2 \cdot H_2O$, where $[Ni(mnt)_2]^+$ is uniformly stacked, intercolumn molecules being connected by hydrogen bonds.[15] This compound shows antiferromagnetic behavior above 100 K which gives $C=0.436$ emu K mol^{-1} and $\theta=-120$ K when fitted by the Curie–Weiss law. Below 100 K inverse susceptibility continuously changes the slope and gives a straight line between 20 and 70 K, which gives $C=0.156$ emu K mol^{-1} and $\theta=+7$ K. Long range ferromagnetic order is observed below 4.9 K in NH_4–$Ni(mnt)_2 \cdot H_2O$. The change from antiferromagnetic to ferromagnetic coupling is interpreted based on McConell's spin polarization theory, which is sensitive to the overlapping mode between the neighboring $Ni(mnt)_2$ molecules.[16] Since the overlapping mode is just in the boundary between antiferromagnetic and ferromagnetic interactions in this compound, a small structural change arising from the structural phase transition alters the antiferromagnetic to ferromagnetic exchange interactions. Although the crystal structure of $(BDNT)_2$–$[Ni(mnt)_2]$ is not known yet, we suppose that BDNT and $Ni(mnt)_2$ have a similar segregated 1D columnar structure, because BDNT is not a planar molecule so that forming a mixed-stack structure may be difficult. The χ^{-1} curve of $(BDNT)_2$–$[Ni(mnt)_2]$ apparently shows the antiferromagnetic to ferromagnetic change around 125 K as well. However, the conductivity plot *vs.* temperature shows no significant anomaly around 125 K. Furthermore, if we analyze the high-temperature region, (150 – 300 K) of this χ^{-1} curve separately from the low-temperature region, in the same way as NH_4–$Ni(mnt)_2 \cdot H_2O$, we obtain a Curie constant which is too large; $C=0.614$ ($N/N_A=1.57$) with $\theta=-46$ K. We therefore consider that this apparent change comes from the T-independent term shown in Table 3. The value of this T-independent term (4.5×10^{-4} emu mol^{-1}) is too large to be regarded as the paramagnetism of BDNT, taking the EPR signal ratio into account. This large value might be ascribed to orbital paramagnetism of Ni but the origin is not clear at the moment. Since the magnetism of $Ni(mnt)_2$ can be understood by the localized spins on $Ni(mnt)_2$, the high electrical conductivity is attributable to the partially oxidized BDNT stack.

In summary, various kinds of charge-transfer salts between BDNT and $M(mnt)_2$ (M = Ni, Pd, Pt, Au) have been obtained, with 2 : 1, 1 : 1, and 1 : 2 chemical compositions. All these salts are conductive (*ca.* 1 S cm^{-1}) with low activation energies, except BDNT–$[Au(mnt)_2]_2$. Among these salts, the coexistence

of ferromagnetic interactions and high conductivity was found in $(BDNT)_2$–$[Ni(mnt)_2]$. BDNT takes part in the high conductivity and $Ni(mnt)_2$ in the ferromagnetic interactions separately. They are well separated and do not interact with each other.

The authors are grateful to Dr. Y. Hosokoshi for fruitful discussions on the magnetic properties of $(BDNT)_2$–$[Ni(mnt)_2]$.

Appendix

Crystal structure of BDNT–$[Au(mnt)_2]_2$

A black octahedral crystal of size 0.2 mm × 0.1 mm × 0.1 mm was mounted on a thin glass capillary with an epoxy resin. X-Ray diffraction intensity data were collected by use of a Rigaku AFC5R four-circle diffractometer with graphite-monochromated Mo-Kα radiation. The intensity data were corrected for absorption. Crystal data and experimental details are given in Table 4. The structure was solved by direct methods and refined by full-matrix least-squares methods. Full crystallographic details, excluding structure factors, have been deposited at the Cambridge Crystallographic Data Centre (CCDC). See Information for Authors, *J. Mater. Chem.*, 1998, Issue 1. Any request to the CCDC for this material should quote the full literature citation and the reference number 1145/61.

The structure of BDNT–$[Au(mnt)_2]_2$ is constituted of twisted non-planar $BDNT^{2+}$ and planar $[Au(mnt)_2]^-$, the dimer of which is stacked along the *c*-axis in a crisscross fashion. The overlap modes within and between the dimer of $Au(mnt)_2$ are shown in Fig. 7(a) and (b) respectively. Contacts shorter than the sum of the van der Waals radii were not found within and between the dimer. A top view of this crisscross column of $Au(mnt)_2$ is shown in Fig. 8(a). BDNT molecules are placed on the centers of symmetry between these columns thus being disordered as shown in Fig. 8(b). Both dithiole rings are twisted *vs.* the central naphthothiadiazole ring, the dihedral angle of which is 54.7° which is close to the

Table 4 Crystal data and experimental details

compound	BDNT–$[Au(mnt)_2]_2$
formula	$C_{24}H_{12}N_2S_5$–$(C_8N_4S_4Au)_2$
crystal system	monoclinic
space group	*C*2/*c*
a/Å	20.861(8)
b/Å	16.175(4)
c/Å	15.032(11)
β/°	115.42(4)
Z	4
$2\theta_{max}$/°	60
radiation	Mo-Kα (*λ* = 0.710 69 Å)
μ(Mo-Kα)/cm^{-1}	70.6
number of reflections used for analysis [$I > 3\sigma(I)$]	2697
number of parameters	326
R, R_w	0.052, 0.045
goodness of fit	1.85
max, min. residual peak/e Å^{-3}	1.6, −2.2

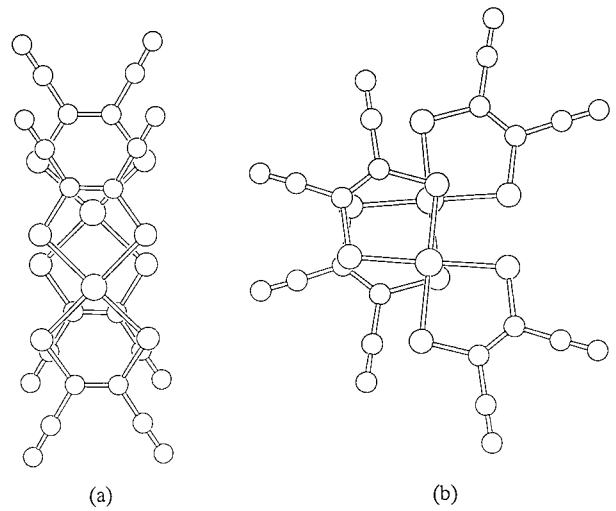

Fig. 7 (a) Intradimer and (b) interdimer overlap modes of $Au(mnt)_2$ in BDNT–$[Au(mnt)_2]_2$

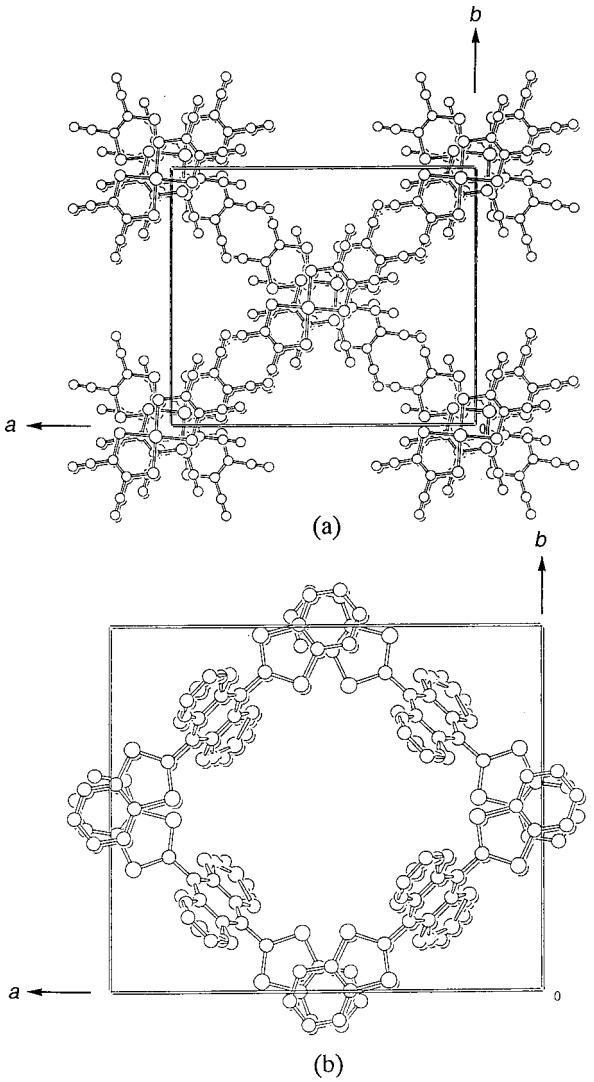

Fig. 8 (a) Top view of the crisscross stack of $Au(mnt)_2$ and (b) $BDNT^{2+}$ orientationally disordered due to the center of symmetry

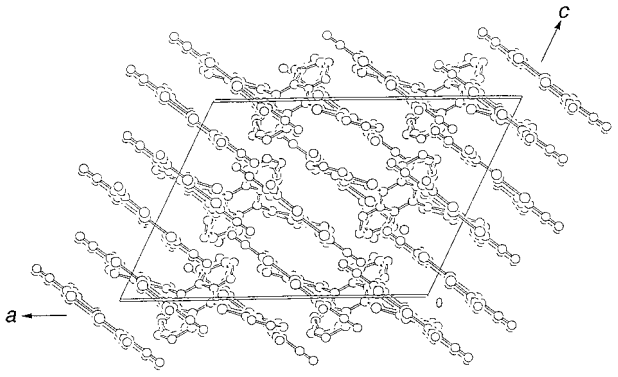

Fig. 9 Side view of the $Au(mnt)_2$ stacks and orientationally disordered $BDNT^{2+}$

corresponding angle (58.7°) of BDNT–$(SbF_6)_2$.[12] This twisted structure is typical of $BDNT^{2+}$. The side view of the $Au(mnt)_2$ columns with $BDNT^{2+}$ is shown in Fig. 9. This crystal structure is consistent with the low electrical conductivity and diamagnetic properties.

References

1 Y. Yamashita, K. Ono, S. Tanaka, K. Imaeda and H. Inokuchi, *Adv. Mater*., 1994, 295.
2 R. Micnas and J. Ranninger, *Rev. Mod. Phys*., 1990, **62**, 113.
3 J. Dong, K. Yakushi and Y. Yamashita, *J. Mater. Chem*., 1995, **5**, 1735.
4 J. Dong, K. Yakushi, Y. Yamashita, K. Imaeda and H. Inokuchi, *Phys. Status Solidi B*, 1996, **195**, 611.
5 P. J. Clemenson, *Coord. Chem. Rev*., 1990, **106**, 171; G. Schmauch, T. Chihara, Y. Wakatsuki, M. Hagiwara and H. Kisch, *Bull. Chem. Soc. Jpn*., 1996, **69**, 2573.
6 R. C. Wheland and I. L. Gilson, *J. Am. Chem. Soc*., 1976, **98**, 3916.
7 L. Alcacer and A. H. Maki, *J. Phys. Chem*., 1974, **78**, 215.
8 R. T. Henriques, L. Alcacer, M. Almeida and S. Tomic, *Mol. Cryst. Liq. Cryst*., 1985, **120**, 237.
9 C. W. Schlapfer and K. Nakamoto, *Inorg. Chem*., 1975, **14**, 1338.
10 S. P. Best, S. A. Ciniawsky, R. J. H. Clark and R. C. S. McQueen, *J. Chem. Soc., Dalton Trans*., 1993, 2267.
11 J. Dong, Thesis, Graduate University of Advanced Studies, 1996.
12 K. Yakushi, J. Dong, M. Uruichi and Y. Yamashita, *Mol. Cryst. Liq. Cryst*., 1996, **284**, 223.
13 G. Ch. Baker Jr., G. S. Rushbrooke and H. E. Gilbert, *Phys. Rev. A*, 1964, **135**, 1272; W. E. Hatfield and K. L. Trojan, *Research Frontiers in Magnetochemistry* ed. C. J. O'Connor, 1993, p. 6.
14 M. L. Allan, A. T. Coomber, I. R. Marsden, J. H. F. Martens, R. H. Friend, A. Charlton and E. E. Underhill, *Synth. Met*., 1993, **55–57**, 3317.
15 P. I. Clemenson, A. E. Underhill, M. B. Hursthouse and R. L. Short, *J. Chem. Soc., Dalton Trans*., 1988, 1689.
16 A. T. Coomber, D. Beljonne, R. H. Friend, J. L. Bredas, A. Charlton, N. Robertson, A. E. Underhil, M. Kurmoo and P. Day, *Nature (London)*, 1996, **380**, 144.

Paper 7/04813K; *Received* 22*nd September*, 1997